# Disturbance Observer-Based Automotive Engine Vibration Isolation Dealing With Non-linear Dynamics and Transient Excitation

Claes Olsson[*†]

April 22, 2005

**Abstract**

Active automotive engine vibration isolation is considered where both stationary and transient engine-induced excitations as well as plant non-linearity are considered.

The adopted control strategy targets the dominating spectral components of the excitation and achieves narrow band vibration isolation using feedback of disturbance states estimates. Time-varying gain-scheduled observer design, including investigations of closed-loop characteristics, is based on a linear parameter varying (LPV) approximation of the considered non-linear engine and subframe suspension system. To generate this representation, an approach of dividing the non-linear system into its linear and non-linear components where the latter is represented using a parameter dependent non-linear function is proposed. Parameter dependent quadratic stability analysis has been made tractable using an affine closed-loop system representation.

High vibration isolation performance is demonstrated using co-simulations incorporating a detailed non-linear plant model and measured engine excitations. This is also achieved for engine operating conditions corresponding to rapid car accelerations, whereas the system exhibits non-linear characteristics and the fundamental frequency of the harmonic disturbance undergoes rapid time variations. Parameter dependent closed-loop quadratic stability is being shown assuming plant linearity. Yet, in the non-linear plant case, stability is guaranteed but only for limited intervals of the parameters and their time derivatives.

**Keywords**

Vibration isolation, non-linearity, transient excitation, gain scheduling, state estimation, quadratic stability

## 1 Introduction

Ideally, an automotive engine suspension system should isolate the engine vibrations caused by the engine internal excitation and, at the same time, prevent excessive engine displacements. This requires frequency dependent dynamic stiffness of the engine suspension elements where the desired stiffness is high at low frequencies and low at higher ones. Conventionally, automotive engine suspension system uses elastomeric and hydraulic engine mounts [1–7] which offer limited possibilities to deal with this contradictory frequency dependence.

To overcome the limitations associated with passive engine suspension elements, active vibration isolation [8] could be adopted. This approach has been given a lot of attention where many solutions have been proposed, some using active engine mounts [2,9–17] and others utilising an alternative isolation strategy based on active absorbers attached to the receiver [18–21].

Apart from a few studies [13,18], most investigations conducted focus on active system performance under stationary or quasi-stationary operating conditions. Furthermore, the consequences on closed-loop stability and performance of non-linear characteristics, also seem to be marginally investigated.

The main objective of this paper is to develop a controller for active automotive engine vibration isolation which could deal with stationary and transient internal engine excitation as well as plant non-linearity. Thus, a control strategy that achieves satisfactory attenuation of the force transmitted to a

[*]This work has been carried out within Volvo Car Corporation's Post Graduate Program in association with Uppsala University, Division of Systems and Control, Dept. of Information Technology.

[†]C. Olsson is with Volvo Car Corporation, Mailing address: Chassis & Vehicle Dynamics, Dept. 96020, PVÖS36, 405 31 Gothenburg, Sweden. Tel.: +46(0)31 3251310; fax: +46(0)591689, Email: colsson5@volvocars.com

flexible subframe, preserves the ability of the open-loop system to prevent large engine displacements, and ensures closed-loop stability for the complete operating range of the plant, is sought. The latter includes engine excitations corresponding to *e.g.* rapid car accelerations where the plant exhibits non-linear characteristics and the fundamental frequency of the engine excitation undergoes rapid time variations.

A similar problem was treated in [15] where gain-scheduled $\mathcal{H}_2$-feedback controllers were utilised for broad band active engine vibration isolation. It was shown that, taking non-linear properties into account could be crucial to achieve closed-loop stability and robust performance. In [17], the widely used time-domain adaptive filtering strategy was, using the system considered in this paper, shown to give insufficient tracking performance when dealing with multiple spectral components of transient excitations corresponding to rapid car accelerations.

The organisation of this paper is as follows. Section 2 presents the considered vibration isolation problem. Next, an approach to generate linear parameter varying (LPV) representations of non-linear systems is described and applied to the considered engine and subframe suspension system in Sections 3 and 4, respectively. Sections 5 and 6 deal with controller design and investigations of the closed-loop characteristics. The results from evaluation of the closed-loop response using co-simulations and measured engine excitations are shown in Section 7. Finally, the paper is concluded in Section 8.

## 2 Statement of the Problem

Figure 1 shows a virtual model of a car engine and its suspension as well as an flexibly suspended flexible subframe. The four cylinder diesel engine is attached to the car body through right- and left-hand side (RHS and LHS) engine mounts, and to the *subframe* via a *torque-rod*. The latter is connecting the engine and subframe using the rubber bushings $B_1$ and $B_2$ while the four rubber bushings, $B_3$-$B_6$, attach the subframe to car body. The engine and subframe suspension system model shown in Figure 1 has been obtained making use of a multi body system (MBS) analysis and simulation software for dynamics [22] where engine and torque-rod are represented as rigid bodies and subframe as a flexible one consisting of six rigid and 24 flexible body modes (using the *Craigh and Bampton* modal synthesis method [23]). This gives a dynamic model with 42 physical and modal degrees of fredom (DOF).

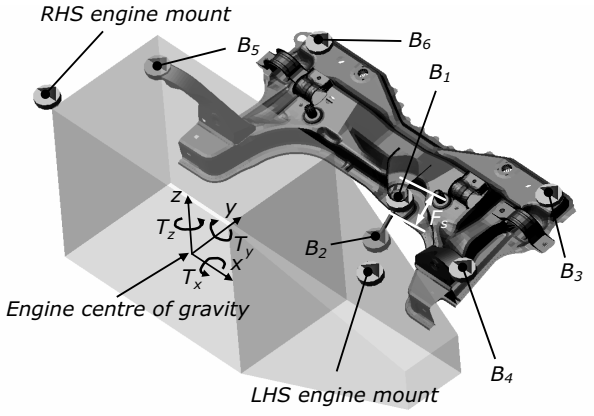


Figure 1: A model of a car engine and subframe suspension system including rigid body engine and gear box, flexible subframe, rigid body torque-rod, six rubber bushings $B_1$-$B_6$, and two engine mounts.

In the model, each engine mount and bushing is represented using 6-DOF (three translational and three rotational) spring and 6-DOF damper elements. The two engine mounts and bushing $B_1$ exhibit non-linear static stiffness characteristics, (Figure 2 (a) presents the non-linear force/displacement characteristics of bushing $B_1$), and linear damping characteristics, while the bushings $B_2$-$B_6$ have linear stiffness and damping characteristics.

The engine is subjected to internal excitation originating from rotating and translating masses and combustion forces. It is assumed to be applied to the engine center of gravity and is represented by the three torques $T_x(t) \in \mathbb{R}^1$, $T_y(t) \in \mathbb{R}^1$, and $T_z(t) \in \mathbb{R}^1$ shown in Figure 1. In addition to the nominal level of the $T_x$-torque, the engine internal excitation is mainly order based which means that for a specific engine speed, its spectral content contains frequency components at frequencies equal to multiples of the

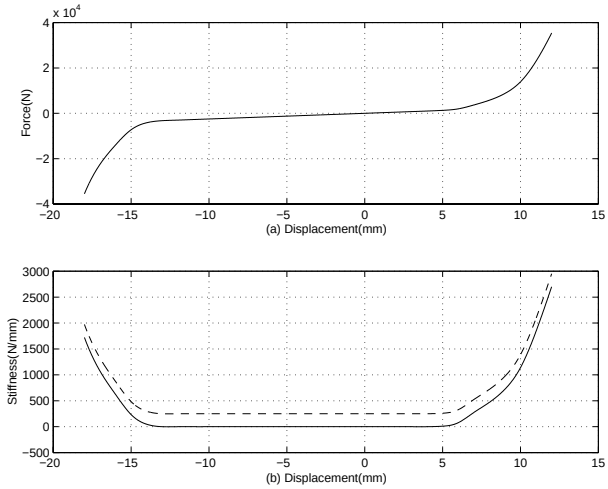


Figure 2: (a) Force/displacement characteristics of bushing $B_1$ in the global $x$-direction. (b) Static translational stiffness function $k(\cdot)$ of bushing $B_1$ in the global $x$-direction (dashed) and the non-linear function $\tilde{k}(\cdot)$ (solid).

rotational engine speed. For convenience the letter 'E' is often used to indicate the engine rotational speed in Hertz. The ignition frequency, i.e. the frequency component at two times the rotational speed for the considered four cylinder engine, is thus referred to as 2E.

Experimental engine internal excitation data has been obtained using twelve simultaneous engine block acceleration measurements (measured at four positions on the engine block in three directions each) followed by *fft* (fast fourier transform)-analysis based on a linearised model of the engine and subframe suspension system. The measurements and, thus, the estimated internal excitation correspond to the following two fundamentally different engine operating conditions

- Idle engine operation
- Car acceleration including a gear shift operation

Figure 3 shows the spectral content of the idling engine $T_y$-torque whereas Figure 4 presents the measured engine speed of rotation for to the acceleration and gear shift operation. In Figure 4, the three vertical lines mark, from the left, start of acceleration running on the 3rd gear, clutch pedal down, and clutch pedal release running on 5th gear. Figure 5 shows the magnitude of a windowed *fft* of the corresponding $T_x$-torque using a sliding window. The nominal level which mainly influences low frequencies is omitted to clearly visualise the characteristics of the $T_x$-torque fluctuations.

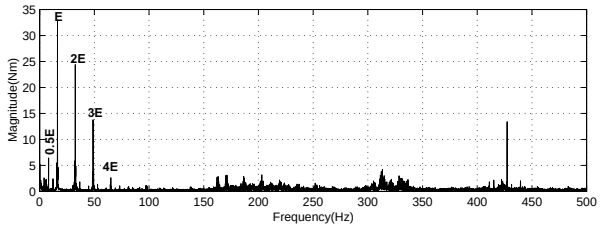


Figure 3: Spectral frequency contents of the $T_y$-torque corresponding to idle engine operation. The five most dominating frequency components have been indicated with reference to the engine speed of rotation as 0.5E, E, 2E, 3E, and 4E.

One of the objectives of engine suspension design is to minimise induced structural vibrations and structure borne noise by limiting the forces transmitted from the engine, to body and to chassis. This contradicts the requirement of preventing large engine displacements within the engine compartment. Since vibration isolation is required essentially for high frequencies, and engine displacements are large only for low frequency excitation, both requirements could be met by separating them with respect to different frequencies. Here, high frequencies refer to frequencies above the highest of the natural

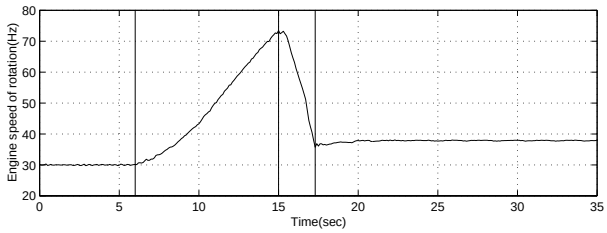


Figure 4: Engine speed of rotation corresponding to an acceleration including a gear shift operation. The three vertical lines mark, from the left, start of acceleration running on the 3rd gear, clutch pedal down, and clutch pedal release running on 5th gear.

frequencies corresponding to the rigid body engine modes. Thus, the engine suspension elements, i.e. engine mounts and bushings, should ideally be designed to have high dynamic stiffness for low frequencies and low one for high frequencies. This is hard to achieve, if not impossible, using passive isolation elements when dealing with premium automotive noise and vibration demands.

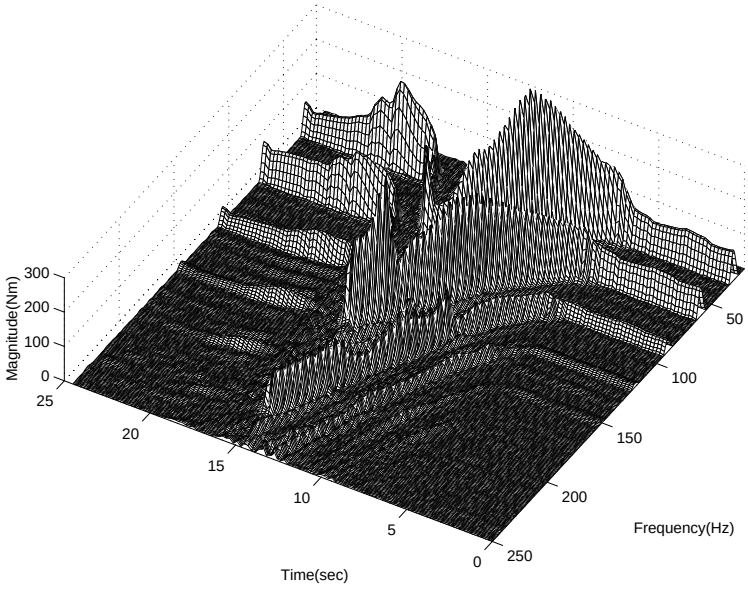


Figure 5: Time-dependent frequency contents of the $T_x$-torque corresponding to the acceleration and gear shift operation.

For the particular engine suspension layout shown in Figure 1 where the front torque-rod bushing $B_2$ is very stiff, the above mentioned frequency dependent dynamic stiffness characteristics are important when considering the rear torque-rod bushing $B_1$. By introducing active isolation technology the isolation performance could be considerably improved.

To actively isolate the engine vibrations from subframe, the bushing $B_1$ connecting torque-rod to subframe is replaced by an actuator consisting of a controllable force in parallel to a *passive stage* with stiffness and damping properties equal to the ones of the removed bushing. The actuator force output is applied in the longitudinal direction of the torque-rod and is indicated $F_A$ in Figure 1 where the doubled arrowed line symbolises force action and reaction. The feedback signal written $F_T(t)$, i.e. the input signal to the controller, is the total transmitted force to subframe in the global $x$-direction. Thus, $F_T(t)$ is the sum of the actuator force output and the force in the passive stage. This choice of feedback measurement has the advantage of low coupling of structure flexibility into the open loop transfer function compared to acceleration sensing [16, 24–26]. This enables the use of a low order model approximation of the plant in controller design and consequently a low order controller.

Thus, the problem addressed in this paper is the one of finding a control strategy for attenuation of the transmitted force $F_T(t)$ when simultaneously dealing with

- effects of the suspension system non-linear characteristics

- engine excitation corresponding to idle and rapid car acceleration operating conditions
- as well as prevention of large engine displacements within the engine compartment

As mentioned above, the engine suspension system considered is a non-linear dynamic system due to non-linear material characteristics. To address stability with respect to plant non-linearity in controller design and to analyse the closed-loop characteristics, an analytical model of the non-linear system is required. For large systems (in terms of number of DOFs), analytical non-linear models representing the non-linear system characteristics are not readily obtained. Therefore, an approach to generate linear parameter varying (LPV) representations of such systems given arbitrarily detailed MBS models is proposed and applied to the considered engine and subframe suspension system.

# 3 An Approach to LPV-modelling of Non-linear Dynamic Systems

The proposed method is based on MBS modelling to generate analytical parameter dependent models of the non-linear dynamic systems. By dividing the system non-linearity into its linear and non-linear components, where the latter is represented using a parameter dependent non-linear function, an LPV-model could be obtained. To elucidate the procedure, a simple 1-DOF mass/spring system shown in Figure 6 (a) is used. The following five steps constitutes the method

1. An arbitrarily detailed MBS model of the non-linear dynamic system to be controlled is generated. The dynamics of this system is described by a first order non-linear differential equation as

$$\dot{x}(t) = g(x(t), d(t)) \tag{1}$$

where $x(t) \in \mathbb{R}^n$ is the state of the system, $d(t) \in \mathbb{R}^m$ is an external disturbance/input, and $g(\cdot)$ is a non-linear function.

2. The non-linear elements to be divided into its components are identified. In Figure 6 (a), this is the spring element whose stiffness $k(l(t))$ depends non-linearly on the displacement $l(t)$ of the mass.

3. The non-linear element is divided into a linear one in parallel to a non-linear parameter dependent element $\widetilde{E}_{NL}(\theta(t))$ which could be written as

$$\widetilde{E}_{NL}(\theta(t)) = E_{NL}(\theta(t))z(t), \quad z(t) = Cx(t) \tag{2}$$

where the parameter $\theta(t) \in \mathbb{R}^p$ is measurable or observable and might depend on the state $x(t)$. Notice that the possibly non-linear matrix function $\widetilde{E}_{NL}(\theta(t))$ must depend linearly on the state of the system. Returning to the 1-DOF system, the non-linear spring in Figure 6 (a) is modelled as a linear one with stiffness $k_0$ in parallel to a force $F_{NL}(t) = (k(l(t)) - k_0)l(t)$. Therefore, $E_{NL}(\theta(t)) = \tilde{k}(t)$ where

$$\begin{aligned} \tilde{k}(t) &= k(l(t)) - k_0 \\ \theta(t) &= l(t) \\ z(t) &= l(t) \end{aligned} \tag{3}$$

4. Consider the non-linear parameter dependent element $E_{NL}(\theta(t))$ as an 'input' and the signal $z(t)$ in (2) as an 'output' and compute a linear (by automatic linearisation [27] about an equilibrium point) state-space model representation as

$$\begin{aligned} \dot{x}(t) &= A_0 x(t) + B_1 E_{NL}(\theta(t))z(t) + B_2 d(t) \\ z(t) &= Cx(t) \end{aligned}$$

5. Finally, the signal $z(t)$ in the dynamic equation is substituted with $z(t) = Cx(t)$. This yields an LPV-model of the non-linear system described by

$$\dot{x}(t) = A(\theta(t))x(t) + B_2 d(t)$$

where $A(\theta(t)) = A + B_1 E_{NL}(\theta(t))C$.

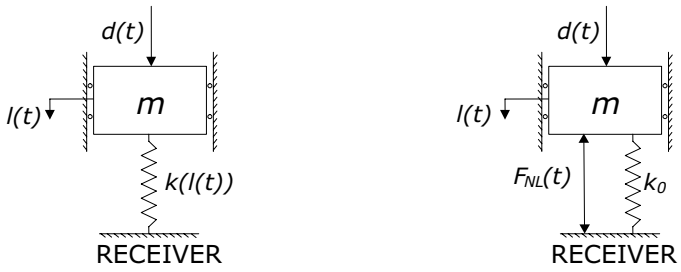


(a) Original non-linear system (b) Equivalent system with divided non-linearity

Figure 6: A 1-DOF mass/spring system used to describe the LPV-modelling approach. The spring has static non-linear stiffness described by the function $k(l(t))$ where its linear and non-linear parts are represented by $k_0$ and the force $F_{NL}(t)$, respectively.

# 4 LPV-modelling of the Non-linear Engine Suspension System

In this study, the non-linear system shown in Figure 1 is simplified by assuming linear stiffness of the two mounts, leaving only one non-linear element, *i.e* the bushing $B_1$. However, it is straightforward to extend the work by introducing further non-linear elements. The input/output relationship corresponding to this non-linear engine and subframe suspension system could be described using a first order non-linear differential equation as

$$\begin{aligned} \dot{x}(t) &= g(x(t), u(t), d(t)) \\ F_T(t) &= h(x(t)) \end{aligned} \tag{4}$$

where $x(t) \in \mathbb{R}^n$, $d(t)$ is the disturbance, *i.e.* $d(t) = \begin{bmatrix} T_x(t) & T_y(t) & T_z(t) \end{bmatrix}^T \in \mathbb{R}^3$, and $u(t) \in \mathbb{R}^1$ is the output of the controller, i.e. the actuator input signal.

Applying the approach outlined in Section 3 to this non-linear system to generate an LVP-model, the non-linear element, i.e. the bushing $B_1$, is treated identically to the non-linear spring in the 1-DOF example system (see Figure 6 (a)). Denote the displacement of the bushing $B_1$ in the global $x$-direction with $l(t)$. The bushing force in this direction depends on $l(t)$ according to the measurements presented in Figure 2 (a). Alternatively, its $x$-directional stiffness could be described using a non-linear function $k(l(\cdot))$ shown as a dashed line in Figure 2 (b). Keeping the notation (3) of the 1-DOF example, an LVP-model of the system (4) is obtained as

$$\begin{aligned} \dot{x}(t) &= A(\tilde{k})x(t) + B_2 d(t) + B_3 u(t) \\ \widetilde{F}_T(t) &= C_3(\tilde{k})x(t) \end{aligned} \tag{5}$$

where

$$\begin{aligned} A(\tilde{k}) &= A_0 + \tilde{k}B_1C \\ &= A_0 + \tilde{k}A_1 \\ C_3(\tilde{k}) &= C(\tilde{k} + k_0) + C_2 \\ &= C_0 + \tilde{k}C_1 \end{aligned} \tag{6}$$

Here, and in the sequel, the dependence of $\tilde{k}(\theta(t))$ on $\theta(t)$ is dropped for notational convenience. In (6), the term $C(\tilde{k}+k_0)$ in the expression for $C_3$ corresponds to the non-linear and linear stiffness contributions to the $B_1$ bushing force and the $C_2$-term to the actuator force output, *i.e.* $F_A(t) = C_2x(t)$.

To emphasise the difference between the characteristics of the non-linear system and one of its linear model approximations, a linear time invariant (LTI) model (7) is introduced by letting $\tilde{k} = 0$ for all $t$ in (5). Thus, the LTI-model (7) corresponds to a linearisation about a static equilibrium position of (4).

$$\begin{aligned} \dot{x}(t) &= A_0x(t) + B_2 d(t) + B_3 u(t) \\ \overline{F}_T(t) &= C_0x(t) \end{aligned} \tag{7}$$

The solid lines in Figure 7 show a Bode diagram of the system (7) from force actuator input $u(s)$ to the total transmitted force $\overline{F}_T(s)$ (here $s$ denotes the Laplace variable). The high frequency roll-off is due to the low-pass characteristics of the actuator.

To validate the accuracy of the LPV-representation (5), simulations have been carried out using the transient excitation load case shown in Figure 5 for the following three models:

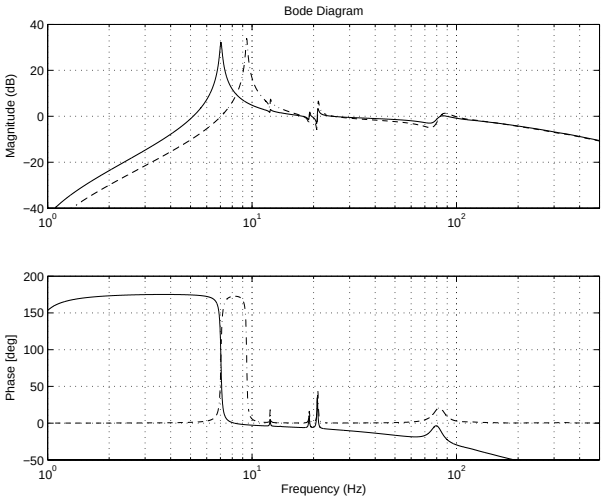


Figure 7: Upper graph shows magnitudes of two transfer functions (relating $u(t)$ to the total force $\widetilde{F}_T(t)$) corresponding to (5) evaluated for $\tilde{k} = 0$ (solid) and $\tilde{k} = 250$ N/mm (dashed). The lower graph presents the phase of the transfer function represented by the solid line in the upper graph (solid), and the phase difference between the two transfer functions shown in the upper graph (dashed).

- The Non-linear model (4) integrated using ADAMS [22]
- The LPV-model (5) integrated using Matlab/Simulink
- The LTI-model (7) integrated using Matlab/Simulink

Figure 8 (a) presents $F_T(t)$ corresponding to the non-linear system (4) and Figure 8 (b) shows the displacement $l(t)$ of the bushing $B_1$ corresponding to the three models. Considering Figure 2, this load case implies operation in the non-linear stiffness region of the bushing $B_1$. The responses of the LPV and the non-linear model show high conformity while the displacement answering to the linear approximation (computed as $l(t) = C_1 x(t)$) deviates substantially. Figure 9 shows $F_T(t)$, $\widetilde{F}_T(t)$, and $\overline{F}_T(t)$ corresponding to the same simulation focusing on two different time intervals for visibility. Both static level and dynamic content of $\widetilde{F}_T(t)$ answers very well to the response $F_T(t)$ of the non-linear model. The linear model (7) offers a poor approximation $\overline{F}_T(t)$ of the total transmitted force $F_T(t)$.

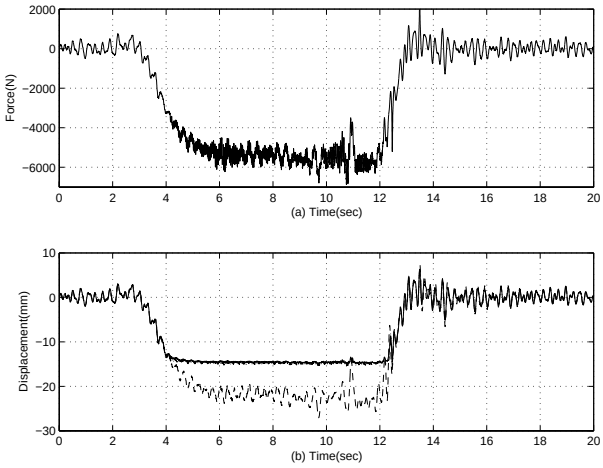


Figure 8: (a) $F_T(t)$ corresponding to the non-linear system (4) subjected to the transient engine excitation. (b) Displacement $l(t)$ of the bushing $B_1$ corresponding to (4) (solid), (5) (dashed), and (7) (dash dotted). Notice that, the dash dotted and solid lines almost coincide.

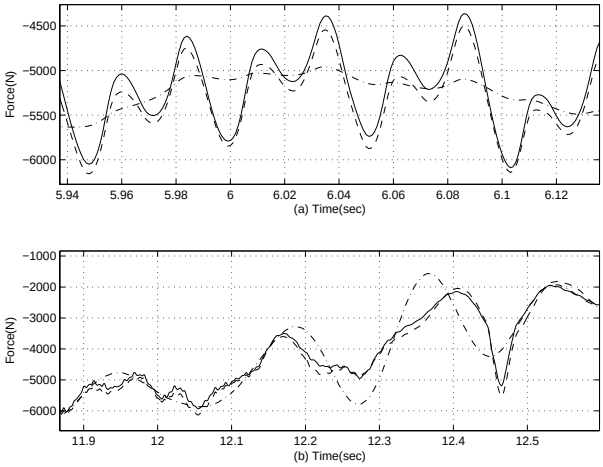


Figure 9: $F_t(t)$ (solid), $\widetilde{F}_T(t)$ (dashed), and $\overline{F}_T(t)$ (dash dotted), corresponding to the simulation results shown in Figure 8 (b).

# 5 Narrow Band Controller Design

The adopted control approach relies on feedback of a disturbance estimate to reject its effect on the total transmitted force. To simplify controller synthesis, the disturbance is modelled as a fictitious additive input signal. Consequently, the plant model is written as

$$\begin{aligned} \dot{x}(t) &= A(\tilde{k})x(t) + B_3 w(t) + B_3 u(t) \\ y(t) &= C_3(\tilde{k})x(t) + n(t) \end{aligned} \tag{8}$$

where $w \in \mathbb{R}^1$ represents the disturbance. The signal $n(t) \in \mathbb{R}^1$ added to the total force output (*i.e.* $y(t) = \widetilde{F}_T(t) + n(t)$) is the output of an autonomous dynamic system given by the following transfer function

$$H_n(s) = C_n(sI - A_n)^{-1}B_n \tag{9}$$

The parameters of this dynamic LTI-filter are used as design parameters to obtain sufficiently low loop gain at low frequencies as well as closed-loop stability.

*Remark 1:* This approach (used in, *e.g*, [18, 28]), where a disturbance model is introduced such that its output completely cancels the disturbance signal without involving the states of the plant in the compensation scheme, is referred to as External Model Control [29].

Due to the engine excitation characteristics, see, for instance, Figures 3 and 5, a few engine orders dominate the spectral contents of the total transmitted force and the lowest frequency component of interest to vibration isolation is order one at engine idle operation, *i.e.* 15 Hz at 900 rpm. To preserve the ability of preventing large engine displacements, the dynamic stiffness has to be left unaffected at frequencies below order one. Thus, assuming slowly varying engine speed of rotation, a controller that stationary achieves high loop gain at the dominating spectral components of the disturbance and low elsewhere is desired.

To capture the order-based characteristics of the disturbance, $w(t)$ is modelled as the output of an autonomous LPV filter as

$$\begin{aligned} \dot{x}_w(t) &= A_w(N(t))x_w(t) \\ w(t) &= [C_{wE} + C_{wDC}]x_w(t) \end{aligned} \tag{10}$$

where $x_w(t) \in \mathbb{R}^{n_w}$, and the time varying matrix $A_w(N(t))$ could be written as $A_w(N(t)) = A_{w0} + N(t)A_{w1}$ for the matrices given by (11).

$$A_{w0} = \begin{bmatrix} Z & 0 & 0 & 0 \\ 0 & Z & 0 & 0 \\ 0 & 0 & Z & 0 \\ 0 & 0 & 0 & \epsilon \end{bmatrix}, \quad A_{w1} = \begin{bmatrix} F & 0 & 0 & 0 \\ 0 & 2F & 0 & 0 \\ 0 & 0 & 3F & 0 \\ 0 & 0 & 0 & 0 \end{bmatrix}$$
$$Z = \begin{bmatrix} -e & 0 \\ 0 & -e \end{bmatrix}, \qquad F = \begin{bmatrix} 0 & 2\pi \\ -2\pi & 0 \end{bmatrix} \tag{11}$$

In (10) and (11), the scalars $e \in \mathbb{R}^1$ and $\epsilon \in \mathbb{R}^1$ are used as design parameters and the vectors $C_{wE}$ and $C_{wDC}$ are given by

$$C_{wE} = [\ 1 \quad 0 \quad 1 \quad 0 \quad 1 \quad 0 \quad 0\ ]$$
$$C_{wDC} = [\ 0 \quad 0 \quad 0 \quad 0 \quad 0 \quad 0 \quad 1\ ]$$

The eigenvalues of $A_w(N)$ are $p_{1,2} = -e \pm 2i\pi N, p_{3,4} = -e \pm 4i\pi N, p_{5,6} = -e \pm 6i\pi N$, and $p_7 = \epsilon$. Thus, $e$ represents the damping of the poles and by choosing $N(t)$ equal to the engine speed of rotation, their imaginary parts could be located to the targeted frequency components of the disturbance $w(t)$, *i.e.* engine orders 1E, 2E, and 3E. In the sequel, $N(t)$ is written $N$ to simplify the notation.

Introducing the augmented state vector $q(t) = [x^T(t) \quad x_w^T(t) \quad x_n^T(t)]^T$ (where $x_n(t) \in \mathbb{R}^{n_n}$ is the state vector of $H_s(s)$ given by (9)) and combining (8), (9), and (10), the plant model used for controller design is now obtained as

$$\begin{aligned} \dot{q}(t) &= A_a(\tilde{k}, N)q(t) + B_{a1}u(t) \\ y(t) &= C_a(\tilde{k})q(t) \end{aligned} \tag{12}$$

where

$$A_a(\tilde{k}, N) = \begin{bmatrix} A(\tilde{k}) & B_3(C_{wE} + C_{wDC}) & 0 \\ 0 & A_w(N) & 0 \\ 0 & 0 & A_n \end{bmatrix}, \quad B_{a1} = \begin{bmatrix} B_3 \\ 0 \\ 0 \end{bmatrix}, \quad C_a^T = \begin{bmatrix} C_3^T(\tilde{k}) \\ 0 \\ C_n^T \end{bmatrix}$$

The states $q(t)$ are estimated by means of a Luenberger observer according to (13). To make the controller given by (13) and (14) independent of $\tilde{k}$, the matrix $A_a$ and the vector $C_a$ are used with $\tilde{k} = 0$ for all $t$.

$$\dot{\hat{q}}(t) = A_a|_{\tilde{k}=0}\hat{q}(t) + B_{a1}u(t) + L(N)(y(t) - \hat{y}(t)) \tag{13}$$

$$u(t) = [\ 0 \quad K \quad 0\ ]\hat{q}(t), \quad \hat{y}(t) = C_a|_{\tilde{k}=0}\hat{q}(t) \tag{14}$$

The control signal is selected as $u(t) = -C_{wE}\hat{x}_w(t)$ to counteract only for the fluctuations of $w(t)$, *i.e.* the spectral components corresponding to the engine orders 1E, 2E, and 3E. Hence, the state feedback gain in (14) is chosen as

$$K = -C_{wE}$$

The observer gain $L(N)$ is computed using gain scheduling based on interpolation of fixed point gains $L_i, i \in \{1, .., m\}$, where $L_i = P(N_i)C_a^T|_{\tilde{k}=0}Q_2^{-1}$ and $P(N_i)$ is the solution to the following algebraic Riccati equation

$$A_a|_{\tilde{k}=0}P(N_i) + P(N_i)A_a^T|_{\tilde{k}=0} + Q_1 + P(N_i)Q_2P(N_i) = 0$$

Using the Riccati equation facilitates the selection of stabilizing observer gains where the matrices $Q_1 \in \mathbb{R}^{(n+n_w+n_n)\times(n+n_w+n_n)}$ and $Q_2 \in \mathbb{R}^{(n+n_w+n_n)\times(n+n_w+n_n)}$ are used as design parameters.

Since the observer has to stabilise the closed-loop system for all possible trajectories of $\tilde{k}$ and $N$, *frozen* stability, *i.e.* stability for constant parameters, is a necessary condition for closed-loop stability. The approach adopted here is to design a $\tilde{k}$-independent controller that makes the closed-loop system stability insensitive to $\tilde{k}$-variations. Motivated by the Nyquist stability criteria [30], this is achieved by keeping the loop gain magnitude far from one at frequencies where $\tilde{k}$ has considerable impact on the plant stationary characteristics.

The determination of frozen stability is based on the poles of the frozen sensitivity function $S(\tilde{k}, N) = (1 - G(s, \tilde{k})F_y(s, N))^{-1}$, where $G(s, \tilde{k})$ is a transfer function representation of (8) evaluated for constant parameter values. Similarly, $F_y(s, N)$ denotes the following controller transfer function

$$F_y(s,N) = [\ 0 \quad K \quad 0\ ](sI - A_a(N)|_{\tilde{k}=0} + B_{a1}[\ 0 \quad K \quad 0\ ] - L(N)C_a|_{\tilde{k}=0})^{-1}L(N) \tag{15}$$

Frozen stability is guaranteed if the poles of $S(\tilde{k}, N)$ have negative real parts for all possible parameter values. To establish frozen stability, interpolation of only two fixed gains $L_0$ and $L_1$ is sufficient for this problem and, thus, the observer gain $L(N)$ is given by

$$L(N) = \alpha L_0 + (1-\alpha)L_1, \quad \alpha = (N - N_1)/(N_0 - N_1) \tag{16}$$

where $N_0$ and $N_1$ represent the minimum and maximum engine speeds of rotation, respectively.

The closed-loop characteristics for stationary parameter values $\tilde{k} = 0$, and $N = 30$ Hz, are illustrated in Figure 10 showing Bode diagrams of the frozen sensitivity function $S(s) = (1 - G(s,\tilde{k})F_y(s,N))^{-1}|_{\tilde{k}=0,N=30}$, of the controller $F_y(s,N)|_{N=30}$, and of the LTI-system $H_n(s)$. The design parameters $e$ and $\epsilon$ are chosen as 0.1 and $-0.1$, respectively. Notice how $H_n(s)$ is used to reduce the controller gain just above 20 Hz, where $\tilde{k}$ has large impact on the plant dynamics which is clear from Figure 7.

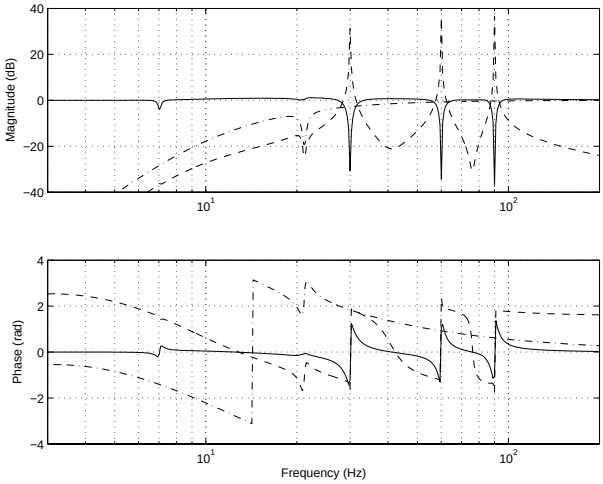


Figure 10: Bode diagrams of the frozen sensitivity function $S(s) = (1 - G(s,\tilde{k})F_y(s,N))^{-1}|_{\tilde{k}=0,N=30}$ (solid), of the controller $F_y(s,N)|_{N=30}$ (dashed), and of $H_n(s)$ (dash dotted).

# 6 Analysis of Closed-loop Characteristics

To facilitate closed-loop stability analysis, a low-pass filter is introduced in the output equation of (8). Hence, this equation is written as

$$y_{lp}(s) = G_{lp}(s)C_3(\tilde{k})x(s) + n(s) \tag{17}$$

where the the transfer function of the LTI low-pass filter $G_{lp}(s)$ is given by

$$G_{lp}(s) = C_{lp}(sI - A_{lp})^{-1}B_{lp} \tag{18}$$

Augmenting the state vector of the observer design model (12) by the state vector $x_{lp}(t) \in \mathbb{R}^{n_{lp}}$ of the low-pass filter $G_{lp}(s)$ and replacing $q(t)$ by $\eta(t) = [x^T(t) \quad x_{lp}^T(t) \quad x_w^T(t) \quad x_n^T(t)]^T$ , the augmented plant could still be described by (12) but for the following matrices and vectors

$$A_a(t) = \begin{bmatrix} A(\tilde{k}) & 0 & B_3(C_{wE} + C_{wDC}) & 0 \\ B_{lp}C_3(\tilde{k}) & A_{lp} & 0 & 0 \\ 0 & 0 & A_w(N) & 0 \\ 0 & 0 & 0 & A_n \end{bmatrix}, \quad B_{a2} = \begin{bmatrix} 0 & 0 \\ 0 & 0 \\ B_w & 0 \\ 0 & B_n \end{bmatrix}$$

$$B_{a1}^T = [\ B_3^T \quad 0 \quad 0 \quad 0\ ]^T, \quad C_a = [\ 0 \quad C_{lp} \quad 0 \quad C_n\ ], \quad D_a = D_n$$

Introducing the state observation error $\tilde{\eta}(t) = \eta(t) - \hat{\eta}(t)$, the closed-loop dynamics are described by the following equation

$$\begin{bmatrix} \dot{x}(t) \\ \dot{\tilde{\eta}}(t) \end{bmatrix} = A_{CL}(\tilde{k}, N) \begin{bmatrix} x(t) \\ \tilde{\eta}(t) \end{bmatrix} \tag{19}$$

In (19), the matrix $A_{CL}(\tilde{k}, N)$ is given by

$$A_{CL}(\tilde{k}, N) = \left[\begin{array}{c|cccc} A(\tilde{k}) & 0 & 0 & -B_3K & 0 \\ \hline \tilde{k}A_1 & A_0 & -L_x(N)C_{lp} & B_3(C_{wE} + C_{wDC}) & -L_x(N)C_n \\ \tilde{k}B_{lp}C_1 & B_{lp}C_0 & A_{lp} - L_{lp}(N)C_{lp} & 0 & -L_{lp}(N)C_n \\ 0 & 0 & -L_{x_w}(N)C_{lp} & A_w(N) & -L_{x_w}(N)C_n \\ 0 & 0 & -L_{x_n}(N)C_{lp} & 0 & A_n - L_{x_n}(N)C_n \end{array}\right] \tag{20}$$

where $L(N)$ has been decomposed as $L(N) = [\ L_x^T(N) \quad L_{x_{lp}}^T(N) \quad L_{x_w}^T(N) \quad L_{x_n}^T(N)\ ]^T$ with block vector dimensions equal to the ones of the corresponding state vectors, *i.e.* $L_x(N) \in \mathbb{R}^n$, $L_{x_{lp}}(N) \in \mathbb{R}^{n_{lp}}$, $L_{x_w}(N) \in \mathbb{R}^{n_w}$, and $L_{x_n}(N) \in \mathbb{R}^{n_n}$.

For the closed-loop dynamics governed by (19), the following stability condition could now be formulated.

**Theorem 6.1** *Consider the matrix-valued function $A_{CL}(\tilde{k}, N)$ in (20) such that $\tilde{k} \in \mathbb{K}$ and $N \in \mathbb{N}$ where $\mathbb{K} = [\tilde{k}_0, \tilde{k}_1]$ and $\mathbb{N} = [N_0, N_1]$. Define the set $\mathbb{P} = \{\wp : (\tilde{k}_0, N_0), (\tilde{k}_0, N_1), (\tilde{k}_1, N_0), (\tilde{k}_1, N_1)\}$. If $\exists P, P > 0$, such that*

$$A_{CL}(\wp)P + PA_{CL}^T(\wp) < 0 \tag{21}$$

*for each $\wp \in \mathbb{P}$, the closed-loop system (19) exhibits exponential stability for all trajectories of $\tilde{k}(t)$ and $N(t)$ within the parameter intervals $\mathbb{K}$ and $\mathbb{N}$, respectively.*

**Proof** Consider the following Lyapunov function

$$V(t) = \begin{bmatrix} x(t) \\ \tilde{\eta}(t) \end{bmatrix}^T P \begin{bmatrix} x(t) \\ \tilde{\eta}(t) \end{bmatrix}, \quad P > 0 \tag{22}$$

Based on *Lyapunov's stability theorem* [31], $\dot{V}(t) < 0$ for all possible state trajectories is a sufficient condition for asymptotic stability [32, 33] of the origin of (19). This could equivalently be expressed as

$$A_{CL}(\tilde{k}, N)P + PA_{CL}^T(\tilde{k}, N) < 0, \quad \forall t \tag{23}$$

The inequality problem (23) has an infinite number of constrains due to the time dependence of the parameters $\tilde{k}(t)$ and $N(t)$. Fortunately, it is sufficient to the check condition (23) at the corners of the parameter box when $A_{CL}(\tilde{k}, N)$ could be written as a fixed function affine in the time-varying parameters $\tilde{k}(t)$ and $N(t)$ where they belong to a convex set [32, 34–36]. Thus, a representation of $A_{CL}(\tilde{k}, N)$ according to (24) is sought.

$$A_{CL}(\tilde{k}, N) = A_{CL}^0 + \tilde{k}A_{CL}^1 + NA_{CL}^2 \tag{24}$$

Due to the low-pass filter $G_{lp}(s)$, the matrix $A_{CL}(t)$ does not contain elements with products of $\tilde{k}(t)$ and $N(t)$ which would otherwise prevented an affine representation to be found. Substituting the expression for $\alpha$ in the expression for $L(N)$ as stated by (16) gives

$$L(N) = \widetilde{L}_0 + N\widetilde{L}_1 \tag{25}$$

where

$$\widetilde{L}_0 = -\frac{N_1L_0 - N_0L_1}{N_0 - N_1}, \widetilde{L}_1 = \frac{L_0 - L_1}{N_0 - N_1}$$

Using the representation (25) of $L(N)$ in (20) and collecting all terms independent of both parameters in $A_{CL}^0$, the terms depending on $\tilde{k}$ in $A_{CL}^1$, and the terms depending on $N$ in $A_{CL}^2$, gives the sought affine representation. The constant matrices of this affine representation (24) are given in the Appendix.

Finally, the theorem follows by noting that for linear systems, asymptotic stability is equivalent to exponential stability [31]. □

*Remark 2:* Theorem 6.1 could be generalised by adopting a less conservative test based on a parameter dependent quadratic Lyapunov function according to (26).

$$\begin{aligned} V(t) &= \begin{bmatrix} x(t) \\ \tilde{\eta}(t) \end{bmatrix}^T (P_0 + \tilde{k}P_1 + NP_2) \begin{bmatrix} x(t) \\ \tilde{\eta}(t) \end{bmatrix} \\ &= \begin{bmatrix} x(t) \\ \tilde{\eta}(t) \end{bmatrix}^T P(\tilde{k}, N) \begin{bmatrix} x(t) \\ \tilde{\eta}(t) \end{bmatrix} \end{aligned} \tag{26}$$

In this case, negative definiteness of the derivative of the Lyapunov function is ensured if

$$A_{CL}(\tilde{k}, N)P(\tilde{k}, N) + P(\tilde{k}, N)A_{CL}^T(\tilde{k}, N) + \dot{P}(\tilde{k}, N) < 0 \tag{27}$$

Since the condition (27) depends on the parameter time variations, bounds on their derivatives have to be introduced. Specifying the derivatives to be contained in a convex set, the fixed structure (26) of $P(\tilde{k}, N)$ together with an affine closed-loop representation allows (27) to be converted to a finite set of LMI constraints [32, 35].

Applying the condition (21) of Theorem 6.1, the stability of the closed-loop system is first investigated under the assumption of plant linearity, *i.e.* assuming that $\tilde{k} = 0$ for all $t$. Using the function *quadstab* implemented in the LMI Control Toolbox [32], the stability condition (21) is checked by solving the following minimisation problem [32]

$$\begin{aligned} &\min \quad \{\tau | A_{CL}(\tilde{k}, N)P + PA_{CL}^T(\tilde{k}, N) < \tau I\} \\ &P > 0 \end{aligned}$$

For the $\tilde{k}$-independent case a negative $\tau$ ($\tau = -2.7 \cdot 10^{-3}$) is achieved for $N(t) \in [30, 80]$ Hz, *i.e.* for engine speeds from 1800 rpm to 4800 rpm where the latter value is near the maximum engine speed of rotation. Thus, for this interval, the closed-loop system possesses global quadratic stability for all possible engine speed time variations. When stability is assessed based on the $\tilde{k}$- and $N$-dependent matrix (20) capturing the actual closed-loop dynamics, exponential stability could still be established but only for small $\tilde{k}$-intervals. Thus, a quadratic Lyapunov function according to (22) seems to be too restrictive to prove closed-loop stability. This is especially true when taking plant non-linearity into account.

To proceed, the existence of a parameter dependent Lyapunov function (27) is investigate using the LMI Control Toolbox function *pdlstab*. Consequently, exponential stability could be proven for the following combinations of parameter intervals and assumptions about the plant characteristics

- $G(s, \tilde{k})|_{\tilde{k}=0, \forall t}$, $N(t) \in [15, 80]$ Hz, $\dot{N}(t) \in [-75, 75]$ Hz/s
- $G(s, \tilde{k})$, $N(t) \in [20, 80]$ Hz, $\tilde{k}(t) \in [0, 250]$ N/mm, $\dot{\tilde{k}}(t) \in [-150, 150]$ N/(mm·s), $\dot{N}(t) \in [-75, 75]$ Hz/s

Figures 11 and 12 show the parameters and their time variations corresponding to the transient excitation load case shown in Figure 5. Thus, considering the plant to be LTI, parameter quadratic stability is guaranteed over the complete engine speed range (see Figure 4) and intervals of the time derivative of the engine speed including *e.g.* maximal accelerations of the car. However, taking plant non-linearity into account, parameter dependent quadratic stability is not sufficient to prove closed-loop stability over the considered plant operating conditions. Without reducing the lower bound on the engine speed interval from the desired 15 Hz to 20 Hz, even more restrictive results were obtained.

*Remark 3:* Considering $A_{CL}(\tilde{k}, N)$ in (20), it is clear that the state estimation error $\tilde{\eta}(t)$ depends on the state feedback gain $K$. Thus, the property of $\mathcal{H}_2$ control usually referred to [30] as the *separation property*, does not apply. This a consequence of neglecting plant non-linearity as determined by $\tilde{k}$ in the state estimation. Consequently, it is not enough to independently establish stability of the plant and of the equations governing the state observation, but the complete matrix $A_{CL}$ of (20) has to be considered.

*Remark 4:* In [18], an equivalent controller structure is adopted to control engine-induced vibrations where the plant is assumed to be captured by an LTI transfer function obtained using least-squares system identification. Motivated by the argument that the parameter $N(t)$ will change slowly, stability is analysed based on the eigenvalues of the $N$-dependent $A$-matrix of the observer, i.e. only frozen stability is considered. In the equivalent case where the non-linearity is neglected, the investigation above presents guaranteed quadratic stability results in addition to frozen stability.

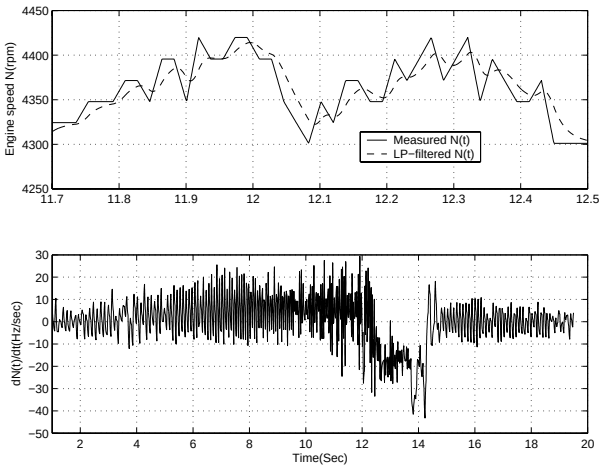


Figure 11: The upper graph presents measured engine speed of rotation (solid) and a low-pass filtered version of it used in the observer implementation (dashed), both corresponding to the transient excitation load case shown in Figure 5. The lower graph shows the time variation of the low-passed filter versions of $N(t)$.

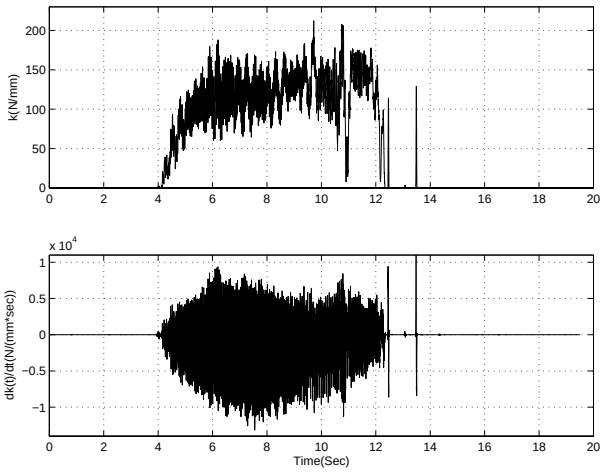


Figure 12: The non-linear stiffness $\tilde{k}(t)$ (upper graph) and its time variation (lower graph) corresponding to the transient excitation load case shown in Figure 5.

# 7 Simulations

The controller presented in Section 5, has been evaluated using the 43-DOF (42 DOFs originating from the control object model plus one DOF from the low-pass characteristic model of the actuator) non-linear plant model (see Figure 1). To present the achieved attenuation of the total transmitted force, the following frequency dependent measure is defined

$$\text{Attenuation}(i\omega) = \frac{|F_T(i\omega)| - |F_{T_0}(i\omega)|}{|F_{T_0}(i\omega)|} \cdot 100 \tag{28}$$

where $F_T(i\omega)$ represents the controlled output and $F_{T_0}(i\omega)$ the corresponding open-loop output, both evaluated using *fft* over sliding windows. Thus, attenuation is the relative change expressed in percentage and -100% means zero transmitted force.

Figure 13 presents the closed-loop response when the plant is subjected to the excitation corresponding to engine idle operation. The three spectral components targeted by the controller are almost completely suppressed, and a good disturbance state estimate is reached rapidly after the controller is turned on at $t = 1$ second.

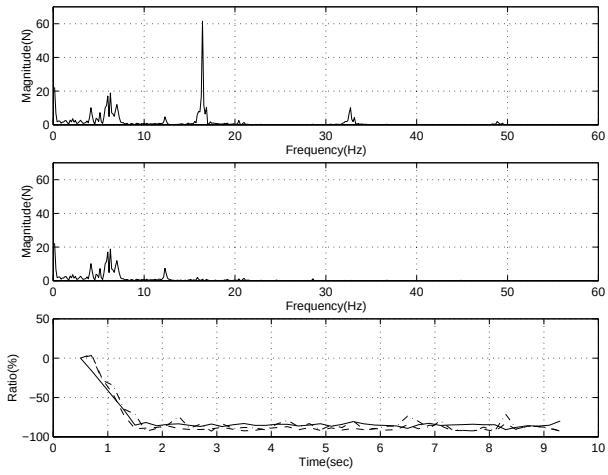


Figure 13: The total transmitted force without control (upper graph) and with control (middle graph), evaluated using *fft* of the signals over the time period $t \in [3, 10]$ seconds where stationary conditions nearly prevails. The lower graph presents the attenuation (as defined by (28)) of the three spectral components: 1E (solid), 2E (dashed), and 3E (dash dotted) targeted by the controller, evaluated using *fft* over a sliding window.

The closed-loop response to the transient excitation is presented in Figures 14 and 15 showing the attenuation of the first and second order of the total transmitted force. Attenuation around -80 % in the acceleration phase and even some under the gear shift maneuver, is achieved. The result for the third order is similar to Figure 15.

Time-dependent frequency contents of the actuator output evaluated using *fft*-analysis over a sliding window is shown in Figure 16. Clearly, the control energy is very much concentrated to the targeted spectral components. It could also be seen that, a substantial control effort is required to deal with the combustion related first order during the rapid car acceleration whereas normal cruising requires rather limited control force magnitudes. Figure 17 presents the actuator force output and demonstrates the satisfactory closed-loop transient response after turning on the controller at $t = 1$ second.

*Remark 5:* In [17], an alternative control strategy based on adaptive filtering using Kalman filter based recursive parameter estimation was investigated for the same plant and measured engine excitations. The tracking achieved using this approach was found insufficient when dealing with excitations corresponding to rapid car accelerations, and the controller had to be switched off during accelerations to avoid amplification of the total transmitted force. Comparing the results of the adaptive filtering approach with the ones corresponding to the observer based strategy considered in this paper, the latter outperforms the one based on adaptive filtering.

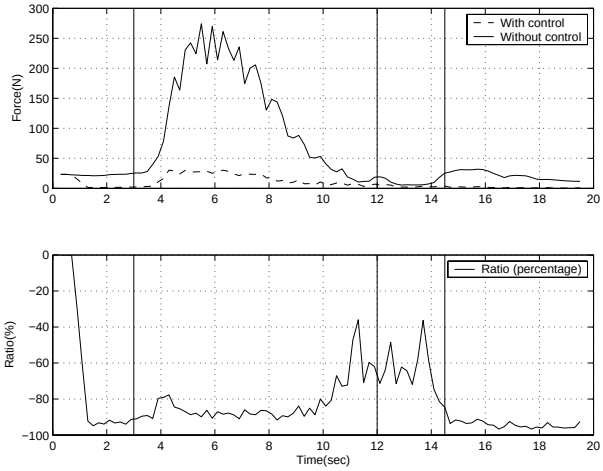


Figure 14: Closed-loop response to the transient excitation evaluated using *fft* of the total transmitted force over a sliding window. The upper graph shows the total transmitted force with (dashed) and without control (solid). The lower graph presents the attenuation of the first order as defined by (28).

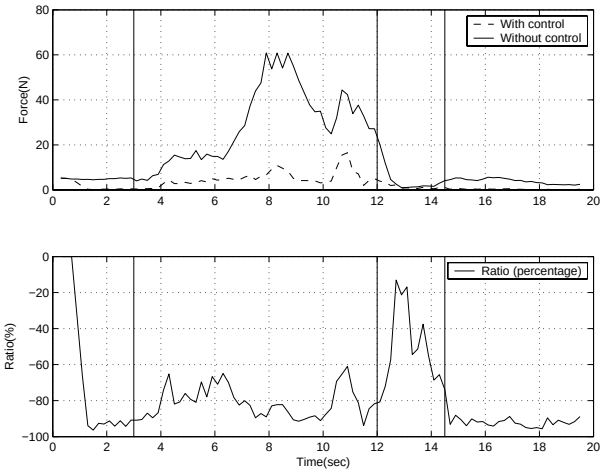


Figure 15: As in Figure 14 but for the second order.

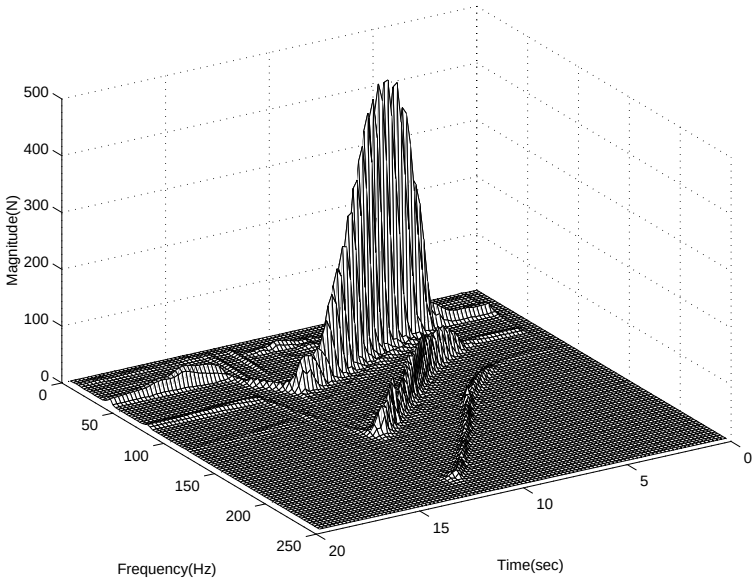


Figure 16: Time-dependent frequency contents of the actuator output corresponding to Figure 14 evaluated using *fft*-analysis over a sliding window.

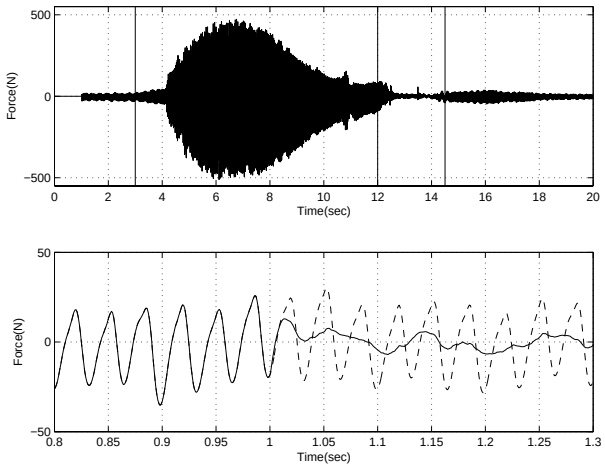


Figure 17: Upper graph shows actuator force output corresponding to the results presented in Figures 14 and 15. The lower graph presents the total transmitted force with (solid) and without control (dashed) illustrating the excellent transient closed-loop response.

# 8 Conclusions

In this work, active automotive engine vibration isolation has been considered dealing with both stationary and transient internal engine excitation as well as plant non-linearity. The plant exhibits non-linear dynamics due to non-linear bushing material characteristics when the engine is subjected to large nominal torques values, which is the case for, *e.g.*, rapid car accelerations. To deal with plant non-linearity, a linear parameter varying (LPV) plant model is derived making use of a novel approach where LPV descriptions of non-linear systems are generated by dividing them into their linear and non-linear components, and the latter is represented using a parameter dependent non-linear function.

The adopted control strategy targets the dominating spectral components of the excitation and attains narrow band vibration isolation using feedback of disturbance states estimates. Sufficient attenuation of the total transmitted force is achieved for both stationary and transient excitations while the ability of the open-loop system to prevent large engine displacements is preserved. This has been demonstrated using co-simulation incorporating a detailed multi body system model and measured engine excitations.

The LPV plant model depends on a parameter representing plant non-linearity whereas the observer is a function of a parameter corresponding to the engine speed of rotation. In addition to frozen stability, which is assured by the controller design, Lyapunov stability is assessed considering time varying parameters. To make quadratic stability analysis tractable, a closed-loop representation affine in the two parameters is derived. Using a parameter dependent quadratic Lyapunov function while neglecting plant non-linearity, exponential stability is shown for wide ranges of engine speeds and their time variations including, *e.g.*, rapid car accelerations. Thus, the adopted approach for closed-loop stability analysis is shown to be useful when dealing with the considered controller strategy for linear time invariant plants. Yet, taking plant non-linearity into account, closed-loop stability has been proven but only for limited intervals of the parameters and their time derivatives. To establish closed-loop stability over the complete plant operating range, further theoretical investigations based on less restrictive stability conditions are required.

# Appendix

The matrices of the affine representation (24) used to assess the stability of the closed-loop system are given by (29), (30), and (31).

$$A^0_{CL} = \left[\begin{array}{c|c|ccc} A_0 & 0 & 0 & -B_3K & 0 \\ \hline 0 & A_0 & \frac{N_1L_{0x}-N_0L_{1x}}{N_0-N_1}C_{lp} & B_3(C_{wE}+C_{wDC}) & \frac{N_1L_{0x}-N_0L_{1x}}{N_0-N_1}C_n \\ 0 & B_{lp}C_0 & A_{lp}+\frac{N_1L_{0lp}-N_0L_{1lp}}{N_0-N_1}C_{lp} & 0 & \frac{N_1L_{0lp}-N_0L_{1lp}}{N_0-N_1}C_n \\ 0 & 0 & \frac{N_1L_{0x_w}-N_0L_{1x_w}}{N_0-N_1}C_{lp} & A_{w0} & \frac{N_1L_{0x_w}-N_0L_{1x_w}}{N_0-N_1}C_n \\ 0 & 0 & \frac{N_1L_{0x_n}-N_0L_{1x_n}}{N_0-N_1}C_{lp} & 0 & A_n+\frac{N_1L_{0x_n}-N_0L_{1x_n}}{N_0-N_1}C_n \end{array}\right] \tag{29}$$

$$A^1_{CL} = \left[\begin{array}{c|cccc} A_1 & 0 & 0 & 0 & 0 \\ \hline A_1 & 0 & 0 & 0 & 0 \\ B_{lp}C_1 & 0 & 0 & 0 & 0 \\ 0 & 0 & 0 & 0 & 0 \\ 0 & 0 & 0 & 0 & 0 \end{array}\right] \tag{30}$$

$$A^2_{CL} = \left[\begin{array}{c|c|ccc} 0 & 0 & 0 & 0 & 0 \\ \hline 0 & 0 & \frac{L_{1x}-L_{0x}}{N_0-N_1}C_{lp} & 0 & \frac{L_{1x}-L_{0x}}{N_0-N_1}C_n \\ 0 & 0 & \frac{L_{1lp}-L_{0lp}}{N_0-N_1}C_{lp} & 0 & \frac{L_{1lp}-L_{0lp}}{N_0-N_1}C_n \\ 0 & 0 & \frac{L_{1x_w}-L_{0x_w}}{N_0-N_1}C_{lp} & A_{w1} & \frac{L_{1x_w}-L_{0x_w}}{N_0-N_1}C_n \\ 0 & 0 & \frac{L_{1x_n}-L_{0x_n}}{N_0-N_1}C_{lp} & 0 & \frac{L_{1x_n}-L_{0x_n}}{N_0-N_1}C_n \end{array}\right] \tag{31}$$


# Acknowledgment

The author would like to thank Prof. Alexander Medvedev of Uppsala University and Dr. Ahmed El-Bahrawy at Volvo Car Corporation for many valuable discussions during the course of this work, and for reading the entire manuscript.

# References


[1] C. B. Nel. Optimmisation of engine mount systems on front-wheel-drive vehicles for multiple operational conditions. In *ISMA25-VOLUME 3*, 2000.

[2] A. Gennesseaux. Research for new vibration isolation techniques from hydro-mounts to active mounts. *SAE Technical Paper 931324*, 1993.

[3] Y. Yu, N. G. Naganathan, and R. V. Dukkipati. A litterature review of automotive vehicle engine mounting systems. MECHANISM AND MASHINE THEORY, 36:123–142, 2001.

[4] M. Müller, U. Weltin, D. Law, M.M Roberts, and T.W. Siebler. The effect of engine mounts on the noise and vibration behaviour of vehicles. *SAE Technical Paper 940607*, 1994.

[5] Y. Yu, N. G. Naganathan, and R. V. Dukkipati. Review of automobile vehicle engine mounting systems. *Int. J. Vehicle Design*, 24(4), 2000.

[6] M. Müller, T. Siebler, and H. Gärtner. Simulation of vibrating vehicle structures as part of the design process of engine mount systems and vibration absorbers. *Society of Automotive Engineers Paper 952211*, 1995.

[7] M. Müller and T. W. Siebler. Methods for the reduction of noise and vibration in vehicles using an appropriate engine mount system. *Society of Automotive Engineers Paper 942414*, 1994.

[8] C. R. Fuller, S. J. Elliott, and P. A. Nelson. *Active Control of Vibration*. ACADEMIC PRESS, 1997.

[9] G. Kim and R. Singh. Engine vibration control using passive, active, and adaptive hydraulic mount systems. *Society of Automotive Engineers Paper 932897*, 1993.

[10] Y. Nakaji, S. Satoh, T. Kimura, T. Hamabe, Y. Akatsu, and H. Kawazoe. Development of an active control engine mount system. *Vehicle System Dynamics*, 32:185–198, 1999.

[11] H. Matsuoka, T. Mikasa, and H. Nemoto. Nv countermeasure technology for a cylinder-on-demand engine - development of active control engine mount. *SAE Technical Paper 2004-01-0413*, 2004.

[12] R. Kashani and A. El-Sinawi. Active engine mount control using a novel kalman estimator-based controller. *SAE Technical Paper 1999-01-1845*, 1999.

[13] A. J. Hillis, A. J. L. Harrison, and D. P. Stoten. A comparison of two adaptive algorithms for the control of active engine mounts. *Journal of sound and vibration*, 2004.

[14] A. M. McDonald, S. J. Elliott, and M. A. Stokes. Active noise and vibration control within the automobile. In *Proceedings of the International Symposium on Active Control of Sound and Vibration, Acoustical Society of Japan, Tokyo*, 1991.

[15] C. Olsson. *Active Engine Vibration Isolation using Feedback Control*. Tekn. Lic. Thesis ISBN = 91-7373-398-9, Division of Automatic Control, Linköping University, Linköping, Sweden, 2002.

[16] C. Olsson. *Structure Flexibility Impacts on Robust Active Vibration Isolation Using Mixed Sensitivity Optimisation*. Technical Report, Department of Information Technology, Uppsala University, Number 2005-003, January 2005.

[17] C. Olsson. *Comparative Study of Recursive Parameter Estimation Algorithms with Application to Active Vibration Isolation*. Technical Report, Department of Information Technology, Uppsala University, Number 2004-051, November 2004.

[18] C. Bohn, A. Cortabarria, V. Härtel, and K. Kowalcyk. Active control of engine-induced vibrations in automotive vehicles using disturbance observer gain scheduling. *Control Engineering Practice*, 12:1029–1039, 2004.

[19] M. Müller, H. G. Eckel, M. Leibach, and W. Bors. Reduction of noise and vibration in vehicles by an appropriate engine mounting system and active absorbers. *Society of Automotive Engineers Paper 960185*, 1996.

[20] H.-J. Karkosch, F. Svaricek, R. A. Shoureshi, and J. L. Vance. *Automotive applications of active vibration control*. In *European Control Conference, Karlsruhe*, 1999.

[21] A. Cortabarria, C. Bohn, J. Hanna, H.-J. Karkosch, P. M. Marienfeld, and F. Svaricek. Design, simulation and implementation of active vibration control systems in automotive vehicles. In *3. VDI/VDE-GMA Aussprachetag Rechnergestutzer Entwurf von Regelungssystem, Dresden*, 2001.

[22] MSC.ADAMS. A registered trademark of MSC.Software Corporation.,2 MacArthur Place, Santa Ana, CA 92707, USA.

[23] M. Gérardin and D. Rixen. *Mechanical Vibrations, Theory and Application to Structural Dynamics, Second Edition*. JOHN WILEY & SONS, 1998.

[24] G. H. Blackwood. *Active Vibration Isolation for Controlled Flexible Structures*. Ph.D. Thesis, Department of Aeronautics and Astronautics, Massachusetts Institute of Technology, 1993.

[25] J. Spanos, Z. Rahman, and A. von Flotow. Active vibration isolation on an experimental flexible structure. In *Proceedings of the SPIE North American Conference on Smart Structures and Intelligent Systems, Albuquerque, New Mexico, SPIE*, volume 1917, pages 674–680, 1993.

[26] B. G. Watters, R. B. Coleman, G. L. Duckworth, and E. F. Bukman. A perspective on an active machinery isolation. In *Proceedings of the 27th Conference on Decision and Control, Austin, Texas*, pages 2033–2038, 1988.

[27] V. N. Sohoni and J. Whitesell. Automatic linearisation of constrained dynamical models. *Transactoins of the ASME, Vol. 108*, September 1986.

[28] A. Medvedev and G. Hillerström. An external model control system. *Control-theory and advanced technology*, 10(4):1643–1665, November 1995.

[29] Tomizuka M., Chew K.-K., and Yang W.-C. Disturbance rejection through an external model. *Transactions of the ASME Journal of Dynamic Systems, Measurements, and Control*, 112:559–564, December 1990.

[30] K. Zhou, J. C. Doyle, and K. Glover. *Robust and Optimal Control*. Prentice Hall, 1996.

[31] H. Khalil. *Nonlinear systems, third edition*. Prentice Hall, 2002.

[32] P. Gahinet, A.J. Laub, and M. Chilali. *LMI Control Toolbox, for Use with MATLAB. The Math Works Inc.*, 1995.

[33] G. Becker, A. Packard, D. Philbrick, and G. Balas. Control of parametrically-dependent linear systems: a single quadratic lyapunov approach. In *Proceedings of the American Control Conference, San Francisco, California*, pages 2795–2799, June 1993.

[34] D. J. Leith and W. E. Leithead. Survey of gain-scheduling analysis and design. *International journal of control*, 73(11):1001–1025, 2000.

[35] F. Bruzelius. *Linear Parameter-Varying System - an approach to gain scheduling*. Ph.D. Thesis, Department of Signals and Systems, Chalmers University of Technology, 2004.

[36] G. Becker and A. Packard. Robust performance of linear parametrically varying systems using parametrically-dependent linear feedback. *Systems & Control Letters*, 10:205–215, 1994.